PHYSICAL REVIEW E **91**, 050601(R) (2015)

Scaling regimes of a semiflexible polymer in a rectangular channel

E. Werner and B. Mehlig*
Department of Physics, University of Gothenburg, Sweden
(Received 25 February 2015; published 14 May 2015)

We derive scaling relations for the extension statistics and the confinement free energy for a semiflexible polymer confined to a channel with a rectangular cross section. Our motivation is recent numerical results [Gupta *et al.*, J. Chem. Phys. **140**, 214901 (2014)] indicating that extensional fluctuations are quite different in rectangular channels compared to square channels. Our results are of direct relevance for interpreting current experiments on DNA molecules confined to nanochannels, as many experiments are performed for rectangular channels with large aspect ratios, while theoretical and simulation results are usually obtained for square channels.

DOI: 10.1103/PhysRevE.91.050601 PACS number(s): 36.20.Ey, 87.14.gk, 87.15.ad

Introduction. Conformations of semiflexible polymers confined to nanochannels are presently intensively investigated since it has emerged that nanochannel confined DNA molecules offer possibilities both for biological applications and as a model system for experimental polymer physics [1–10]. These studies, and the theoretical and simulation results which have accompanied them, have shown that semiflexible polymers such as DNA exhibit a much richer spectrum of behaviors under confinement than do flexible polymers [11–16].

Since it is convenient to fabricate nanochannels with a fixed height but varying widths, many experimental studies [1–5,8,17–19] of confined DNA are performed in rectangular channels (width D_W, height D_H) with aspect ratios far from unity, $D_W \gg D_H$. However, most simulation and theoretical studies [5,12–16,20–22] are restricted to channels with square cross sections, $D_W = D_H$. A common procedure is to analyze the experimental results in terms of the "effective channel size" $\sqrt{D_W D_H}$, simply disregarding the influence of the aspect ratio.

Recently, Gupta *et al.* [8] have shown that the variance of the extension of the DNA molecule does depend on the aspect ratio, but a theoretical explanation for this intriguing result is lacking. This motivated us to analyze how the aspect ratio influences the extension statistics of confined semiflexible polymers. At first sight this appears to be a difficult problem, because it is governed by a large number of length scales: the contour length L of the polymer, its effective width w, its Kuhn length ℓ_K [23], its global persistence length g (the orientational correlation length of the confined chain, defined in Refs. [11,16]), the typical contour-length separation between intrachain collisions l_{cc}, the typical contour-length separation between collisions with the floor and the ceiling of the channel l_{ch}, the typical contour-length separation between collisions with the vertical walls of the channel l_{cw}, and the channel width D_W and height D_H. There are many different confinement regimes corresponding to different orderings of these length scales, potentially resulting in a very complicated phase diagram (Fig. 1). Little is known about this phase diagram for rectangular channels, except in the limit of very strong confinement [11,24,25]. To interpret a given experiment it is necessary to determine which regime in the phase diagram it corresponds to, and what the resulting scaling relations for the extension statistics are.

In this Rapid Communication we summarize the results of our analysis, based on the mean-field theory for the extension of an unconfined semiflexible polymer [26]. It is well known how this theory must be adapted to describe the extension of semiflexible polymers confined to square channels with $D_W = D_H \equiv D$ [11]: for a wide channel and a long polymer, the polymer is divided into a series of spherical blobs of size D. One assumes that mean-field scaling holds for each blob and concludes that the extension of the confined polymer scales as $D^{-2/3}$. We generalize this analysis to rectangular channels. To this end it is necessary to consider a hierarchy of blobs (inset of Fig. 1). For the special case of a flexible chain, this approach was used by Turban to compute its extension in a rectangular channel [27]. We emphasize that this is a much simpler problem since a flexible chain exhibits only a single confinement regime, as opposed to the semiflexible polymer, as pointed out above.

An important result of our analysis is that the scalings can be simply summarized, despite the fact that the phase diagram Fig. 1 exhibits many different regimes. First, we find that the average extension is approximately independent of channel aspect ratio, provided that at least one of the channel dimensions is significantly larger than the Kuhn length of the polymer. This is an important finding because it implies that it is reasonable to analyze the average extension of nanoconfined DNA molecules in terms of the effective channel size $\sqrt{D_W D_H}$. Second, we find that the extension variance depends strongly on both channel dimensions separately; it would be incorrect to analyze it in terms of the effective channel size. We find that the variance increases rapidly as the aspect ratio increases far beyond unity. Our theoretical results for the variance explain the findings of Ref. [8]; they also make it clear that square channels are much preferred for applications where extensional fluctuations are required to be as small as possible. Third, we compute the free energy of confinement; it is approximately determined by the smallest confining dimension. These scaling predictions were derived under the mean-field approximation of Flory [26], but in certain parameter regimes (regimes IIa and IIb in Fig. 1), the results are supported by an asymptotically exact theory that was developed for square channels [22], but can be generalized to rectangular channels.

We have summarized these results in a table in the Supplemental Material [28], also including results for very

*Bernhard.Mehlig@physics.gu.se

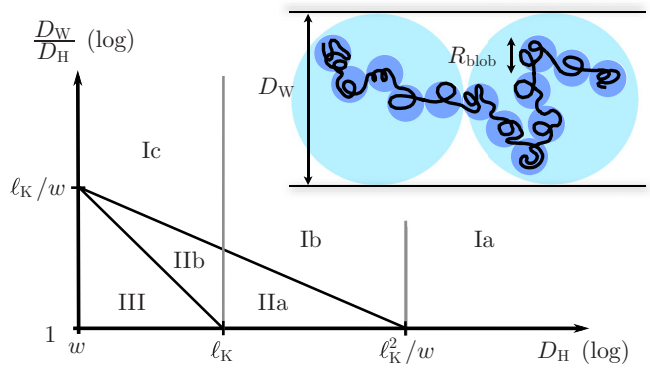

FIG. 1. (Color online) Phase diagram of different scaling regimes for the extension statistics of a semiflexible polymer confined to a channel with a rectangular cross section. The scaling in regime I is given by Eqs. (7) and (8). The scaling in regime II is given by Eqs. (16) and (17). The vertical gray lines distinguish different scaling regimes of the confinement free energy (see text). Results for regime III have been derived elsewhere [11,16,24,25] and are discussed in the Supplemental Material [28]. Inset: An illustration of the hierarchy of blobs analyzed in regime I. In regime Ia, the smaller blobs are spherical blobs of size $R_{blob} \approx D_H$. In regimes Ib and Ic they are cylindrical, of height D_H and width $R_{blob} > D_H$.

strong confinement that were derived by other authors. For other observables (e.g., dynamics, statistics of circular polymers, probability of knot formation), the scaling properties remain to be determined, but the distinctions between the regimes we derive here must also apply to them.

Method. We assume that the polymer is described by the self-avoiding wormlike chain model [23] with Kuhn length ℓ_K and effective width $w < \ell_K$. The centerline of the polymer is confined to a rectangular channel of height D_H and width $D_W \geqslant D_H$. We analyze the conformational fluctuations of the confined polymer in terms of a hierarchy of blobs assuming that the self-avoiding random walks obey Flory's mean-field theory [26] in two and three spatial dimensions. To summarize this theory, assume that the polymer consists of N independent segments of length ℓ and excluded volume v. In $d = 2,3$ dimensions the mean-field result for the average of the extension R of the polymer is [26]

$$R \approx (N^3 \ell^2 v)^{1/(d+2)}. \tag{1}$$

Here the symbol $\approx$ indicates a scaling relation, ignoring factors of order unity. The variance of the extension is determined by self-similarity. The self-avoiding polymer in two or three dimensions has only one macroscopic length scale (R) [23]. Thus, the standard deviation of the extension must scale as the average extension [29]:

$$\sigma_R \approx R \approx (N^3 \ell^2 v)^{1/(d+2)}. \tag{2}$$

As we show below, the analysis of the extension statistics of the confined polymer must proceed by different steps, depending on the relation between the contour-length scales $\ell_K, g, l_{cc}, l_{ch}, l_{cw}$, defined in the Introduction. The global persistence length g only differs appreciably from the Kuhn length ℓ_K at very strong confinement (regime III in Fig. 1). Theories for this regime have been derived elsewhere [11,16,24,25], and are briefly discussed in the Supplemental Material [28].

Extension statistics. Consider the separation of scales

$$\ell_K \ll l_{cc} \ll l_{ch} \ll l_{cw} \ll L. \tag{3}$$

How do the average extension and its standard deviation depend upon D_W and D_H? Since $l_{cc} \ll l_{ch}$, the polymer exhibits three-dimensional Flory scaling before its first collision with the channel walls. The first collision with the ceiling or the floor must occur when a section of contour length l_{ch} has formed a spherical Flory blob of diameter D_H. Applying Eq. (1) with $N = l_{ch}/\ell_K$, $\ell = \ell_K$ and $v \approx \ell_K^2 w$ [30] yields

$$D_H \approx \left(l_{ch}^3 v/\ell_K\right)^{1/5} \Leftrightarrow l_{ch} \approx \left[D_H^5/(\ell_K w)\right]^{1/3}. \tag{4}$$

The resulting blobs perform a two-dimensional self-avoiding walk until they have formed a circular "superblob" of diameter D_W (we follow the terminology of Ref. [27]). This two-dimensional random walk is illustrated in the inset of Fig. 1. The number of small spherical blobs constituting one superblob can be estimated from Eq. (1) with $d = 2$, and $\ell = D_H$ since each small spherical blob constitutes an independent segment of the walk. We assume that the small blobs do not overlap, thus the two-dimensional excluded area of the random walk of small blobs approximately equals the area of a circle of diameter D_H; in other words, $v \approx D_H^2$ in this context. Equation (1) results in

$$D_W \approx \left(N_{blobs}^3 D_H^4\right)^{1/4} \Leftrightarrow N_{blobs} \approx (D_W/D_H)^{4/3}. \tag{5}$$

The contour length stored within a superblob equals l_{cw},

$$l_{cw} \approx N_{blobs} l_{ch} \approx \left[D_W^4 D_H/(\ell_K w)\right]^{1/3}. \tag{6}$$

There are L/l_{cw} superblobs that line up along the channel [Fig. 1 (inset)]. Each superblob has average diameter D_W with fluctuations of the same order. The average extension and its fluctuations are therefore given by

$$R \approx (L/l_{cw}) D_W \approx L[\ell_K w/(D_H D_W)]^{1/3}, \tag{7}$$

$$\sigma_R^2 \approx (L/l_{cw}) D_W^2 \approx L\left(\ell_K w D_W^2/D_H\right)^{1/3}. \tag{8}$$

Equation (7) was recently derived in Ref. [31], but without specifying under which conditions the derivation is valid. We now answer this question. The inequality $l_{cc} \ll l_{ch}$ requires that ideal scaling within a blob of size D_H results in a large number of intrachain collisions within the blob

$$(D_H/\ell_K)^4 v/D_H^3 \approx D_H w/\ell_K^2 \gg 1 \Leftrightarrow D_H \gg \ell_K^2/w. \tag{9}$$

This corresponds to regime Ia in Fig. 1.

The inequality $l_{cw} \gg l_{ch}$ is satisfied if $D_W \gg D_H$. However, the scaling relations (7) and (8) reproduce exactly the well-known relations for square channels as the limit $D_W \to D_H$ is taken, commonly referred to as "de Gennes scaling" [32]. Thus de Gennes scaling for square channels is simply a special case of the more general scaling relations derived above for rectangular channels. Yet attempting to generalize from square to rectangular channels by simply replacing D by the geometrical average $(D_H D_W)^{1/2}$ gives the wrong prediction for the variance of the extension, as Eq. (8) shows.

Now consider a different ordering of length scales:

$$\ell_K \ll l_{ch} \ll l_{cc} \ll l_{cw} \ll L. \tag{10}$$

This corresponds to $D_H \ll \ell_K^2/w$, while D_W remains large (regime Ib in Fig. 1). Are the scaling relations (7) and (8) modified in this regime? Since $l_{ch} \ll l_{cc}$, the polymer must exhibit ideal scaling even after the first collision with the ceiling or the floor of the channel. This scaling persists approximately until the first intrachain collision, which occurs after a contour length l_{cc}. This length scale is estimated by assuming that such a section of the polymer will form a cylindrical blob with height D_H and diameter $R_{blob} \approx \sqrt{l_{cc}\ell_K}$, and by setting the expected number of collisions within the blob to unity:

$$\frac{(l_{cc}/\ell_K)^2\ell_K^2 w}{R_{blob}^2 D_H} = \frac{l_{cc} w}{\ell_K D_H} \approx 1 \Leftrightarrow l_{cc} \approx \frac{\ell_K D_H}{w}. \quad (11)$$

These blobs perform a two-dimensional self-avoiding walk until the first collision with the sidewalls [Fig. 1 (inset)]. Flory scaling for the $N = l_{cw}/l_{cc}$ blobs of size $\ell \approx R_{blob} \approx \sqrt{l_{cc}\ell_K}$ and excluded area $v \approx R_{blob}^2 \approx l_{cc}\ell_K$ yields

$$l_{cw} \approx \left[D_W^4 D_H / (\ell_K w)\right]^{1/3}. \quad (12)$$

This is the same as in regime Ia, Eq. (6). From this point, the derivation of the extension statistics follows that of regime Ia. We infer that the scalings, Eqs. (7) and (8), hold also in regime Ib.

Further decreasing D_H below ℓ_K one enters a different regime (labeled Ic in Fig. 1). It corresponds to this ordering of length scales:

$$l_{ch} \ll \ell_K \ll l_{cc} \ll l_{cw} \ll L. \quad (13)$$

In this case the polymer runs almost completely parallel to the floor of the channel but can otherwise rotate freely. While the expression for the excluded volume of a Kuhn length segment must change because of confinement, the scaling $v \approx \ell_K^2 w$ still holds. To see this, consider two Kuhn length segments. Although they undulate slightly in the vertical direction according to Odijk's theory [11], the segments are always almost horizontally aligned. Consider the two-dimensional projection of these segments, where the vertical direction has been projected out. Assuming that these projections overlap, the probability that the segments overlap in three-dimensional space is approximately w/D_H. Thus, the excluded volume is given by $v \approx wA$, where $A \approx \ell_K^2$ is the excluded area of the two-dimensional projections [30]. The result $v \approx \ell_K^2 w$ follows. Now, exactly the same steps as in the derivation of the extension statistics in regime Ib can be carried out in this regime, leading to identical scaling predictions [Eqs. (7) and (8)]. The prefactors differ between the regimes, however.

Since the steps in the above derivation are different between regime Ia and regimes Ib and Ic, it is at first glance surprising that the scaling predictions for the extension are identical for these regimes. But note that the scaling analysis is formulated in terms of blobs that obey Flory's mean-field scaling. As long as mean-field theory is used throughout, the final prediction for the extension must be independent of the way in which the blobs are arranged. Since in mean-field theory the repulsive effect of self-avoidance is directly determined by the number of monomers within the volume spanned by the polymer, this also explains why the scaling of the extension is a function of the cross section only, independent of the aspect ratio of the channel.

What about the variance of the extension? Combining mean-field theory with the universality of self-avoiding random walks [29] shows that the contour length contained in one superblob [Fig. 1 (inset)] is identical for these regimes, and that each blob experiences size fluctuations of order D_W. The variance of the extension is given by summing the variances of each blob, yielding $\sigma_R^2 \approx N_{superblobs} D_W^2 \approx L(\ell_K w D_W^2/D_H)^{1/3}$. Thus the variance increases as the aspect ratio increases. This demonstrates that rectangular channels are in fact quite different from square ones in this regime.

If the excluded volume of the polymer is so small that the polymer experiences multiple collisions with sidewalls, floor, and ceiling between each intrachain collision, then we obtain different scaling relations. Consider the following ordering of length scales:

$$\ell_K \ll l_{ch} \leqslant l_{cw} \ll l_{cc} \ll L. \quad (14)$$

Under these conditions the polymer obeys ideal scaling until a blob forms that fills the channel cross section, and is further elongated along the channel direction, until it reaches an extension $R_{blob} \approx \sqrt{l_{cc}\ell_K}$. From ideal scaling it follows that $l_{ch} \approx D_H^2/\ell_K$ and $l_{cw} \approx D_W^2/\ell_K$. The length scale l_{cc} is estimated in a similar way as Eq. (11) is obtained:

$$\frac{(l_{cc}/\ell_K)^2\ell_K^2 w}{R_{blob} D_H D_W} \approx 1 \Leftrightarrow l_{cc} \approx \left(\frac{\ell_K D_H^2 D_W^2}{w^2}\right)^{1/3}. \quad (15)$$

The conditions of Eq. (14) thus correspond to $\ell_K \ll D_H \leqslant D_W \ll (D_H\ell_K^2/w)^{1/2}$ (regime IIa in Fig. 1). In this regime, the polymer arranges itself into a line of L/l_{cc} blobs of size R_{blob}:

$$R \approx (L/l_{cc})R_{blob} \approx L[\ell_K w/(D_H D_W)]^{1/3}, \quad (16)$$

$$\sigma_R^2 \approx (L/l_{cc})R_{blob}^2 \approx L\ell_K. \quad (17)$$

We see that the scaling of the average extension agrees with Eq. (7). The reason is that both equations were derived assuming mean-field statistics within each blob, and as noted above, the ordering of the blobs does not influence the prediction for the average extension. However, note that the scaling of the standard deviation, Eq. (17), differs from Eq. (8). We see that σ_R does not depend upon either D_W, D_H, or w.

For the special case of square channels, regime IIa has been studied under the name "extended de Gennes regime" [12,14,21,22]. Figure 1 shows that the limits of this regime are more restrictive for rectangular than for square channels: even if a square channel with side length either D_H or D_W is in regime IIa, the rectangular channel with side lengths D_H and D_W may not be.

Finally, consider the ordering of length scales

$$l_{ch} \ll \ell_K \ll l_{cw} \ll l_{cc} \ll L, \quad (18)$$

corresponding to $D_H \ll \ell_K \ll D_W \ll (D_H\ell_K^2/w)^{1/2}$. This regime is denoted as IIb in Fig. 1. The steps needed to derive the scaling relations for the extension are identical to those summarized above, and again lead to Eqs. (16) and (17), albeit with different prefactors than for regime IIa. The scaling for the extension in regime IIb was previously derived by Odijk [11].

Comparison with results of computer simulations. Our results give a qualitative explanation for the surprising observation of Gupta *et al.* [8], who found in simulations that while the average extension of a confined polymer was relatively insensitive to the aspect ratio of the confining channel, the variance increased with aspect ratio (see Fig. 5 in Ref. [8]). They performed simulations and experiments with a fixed channel height $D_H = 100$ nm and channel widths in the range $D_W = 100$–1000 nm, and compared these against simulations of square channels with matching effective channel size. For their simulations, they used a polymer with $\ell_K = 137.4$ nm and $w = 18.7$ nm. Thus, while the square channels are all approximately in regime IIa, the channels with fixed height cross over into regime Ib as the aspect ratio increases significantly above unity (Fig. 1). While our prediction for mean extension shows the same scaling in these regimes, the variance is independent of D_H and D_W in regime IIa but increases as $D_W^{2/3}$ in regime Ib, qualitatively explaining the results of Gupta *et al.* That the agreement is only qualitative is not surprising, considering that the conditions for regime Ib are only marginally satisfied, and that the contour length of λ-DNA which their simulations mimic is not quite long enough to enter the asymptotic regime where $R \propto L$ [8].

Accuracy of mean-field theory. The results that we derived for regimes I and II are based on Flory's mean-field theory. This theory is thought to be correct in two dimensions but is known to be only approximate in three dimensions [33]. Using the scaling $R \propto L^{0.588}$ in three dimensions would lead to modified scaling predictions for regime Ia (but not for the other regimes): $R \propto D_H^{-0.37} D_W^{-1/3}$, $\sigma^2 \propto D_H^{-0.37} D_W^{2/3}$ (and $F_c \propto D_H^{-1.70}$, see below).

For square channels in regime IIa, we have recently shown both that the scalings of mean-field theory are exact in this regime, and that there are rigorous bounds for the prefactors [22]. These results were derived by mapping the statistics of the extended de Gennes regime to a one-dimensional model known as the weakly self-avoiding random walk. Since the same mapping can be performed for rectangular channels, these exact results are valid throughout regime IIa. The scalings of Eqs. (16) and (17) can thus be rigorously proven. The rigorous bounds for the prefactors are included in the table in the Supplemental Material [28]. As in regime IIa, it is in principle possible to map the statistics of regime IIb to a solved one-dimensional model. The existence of the mapping shows that also in this regime, the scalings of the extension statistics are exact. Computing the exact parameters of the mapping would require performing an integral over the monomer density profile in the Odijk regime, which we have not attempted.

Free energies. Apart from the statistics of the extension, the free energy of confinement F_c is of experimental relevance, as it determines the force that must be applied to introduce a polymer into a channel. For the polymer confined to a channel, this free energy can be estimated by kT times the number of collisions with the walls, or

$$F_c/(kT) \approx L/l_{ch} + L/l_{cw} \approx L/l_{ch}. \tag{19}$$

For regime Ia, we obtain a scaling prediction for F_c by inserting Eq. (4) into Eq. (19), yielding $F_c \approx L(\ell_K w/D_H^5)^{1/3}$. For all other regimes, the free energy of confinement agrees with known results for ideal polymers [24,34], with the agreement becoming exact in the asymptotic limit where the inequalities defining the respective regimes are perfectly satisfied. These predictions for F_c are included in the table in the Supplemental Material [28].

Conclusions. Recent experiments on DNA in rectangular nanochannels are performed at high aspect ratio, yet most analytical and simulation results pertain to square channels. These analytical results are often applied to rectangular channels by matching the cross-sectional area of the rectangular channel to that of the square one. Our theory shows that this matching allows one to predict the average DNA extension under fairly general assumptions. We also show that this procedure fails to correctly predict the scalings of other observables, such as the variance. Our theory explains recent numerical results for the extension variance in rectangular channels [8], and shows that square channels are most useful for biological applications where it is beneficial that the extension variance is small. We expect that the results summarized here can be generalized to other observables, such as the statistics of circular DNA, knot formation, and DNA dynamics [3,35].

Acknowledgments. Financial support from Vetenskapsrådet and from the Göran Gustafsson Foundation for Research in Natural Sciences and Medicine is gratefully acknowledged.

[1] J. O. Tegenfeldt, C. Prinz, H. Cao, S. Chou, W. W. Reisner, R. Riehn, Y. M. Wang, E. C. Cox, J. C. Sturm, and P. Silberzan, Proc. Natl. Acad. Sci. USA **101**, 10979 (2004).

[2] W. Reisner, K. J. Morton, R. Riehn, Y. M. Wang, Z. Yu, M. Rosen, J. Sturm, S. Y. Chou, E. Frey, and R. H. Austin, Phys. Rev. Lett. **94**, 196101 (2005).

[3] C. H. Reccius, J. T. Mannion, J. D. Cross, and H. G. Craighead, Phys. Rev. Lett. **95**, 268101 (2005).

[4] F. Persson, P. Utko, W. Reisner, N. B. Larsen, and A. Kristensen, Nano Lett. **9**, 1382 (2009).

[5] E. Werner, F. Persson, F. Westerlund, J. O. Tegenfeldt, and B. Mehlig, Phys. Rev. E **86**, 041802 (2012).

[6] W. Reisner, J. N. Pedersen, and R. H. Austin, Rep. Prog. Phys. **75**, 106601 (2012).

[7] J. J. Jones, J. R. C. van der Maarel, and P. S. Doyle, Phys. Rev. Lett. **110**, 068101 (2013).

[8] D. Gupta, J. Sheats, A. Muralidhar, J. J. Miller, D. E. Huang, S. Mahshid, K. D. Dorfman, and W. Reisner, J. Chem. Phys. **140**, 214901 (2014).

[9] M. Alizadehheidari, E. Werner, C. Noble, M. Reiter-Schad, L. K. Nyberg, J. Fritzsche, B. Mehlig, J. O. Tegenfeldt, T. Ambjörnsson, F. Persson, and F. Westerlund, Macromolecules **48**, 871 (2015).

[10] W. F. Reinhart, J. G. Reifenberger, D. Gupta, A. Muralidhar, J. Sheats, H. Cao, and K. D. Dorfman, J. Chem. Phys. **142**, 064902 (2015).

[11] T. Odijk, Phys. Rev. E **77**, 060901 (2008).

[12] Y. Wang, D. R. Tree, and K. D. Dorfman, Macromolecules **44**, 6594 (2011).

[13] D. R. Tree, Y. Wang, and K. D. Dorfman, Phys. Rev. Lett. **108**, 228105 (2012).
[14] L. Dai and P. S. Doyle, Macromolecules **46**, 6336 (2013).
[15] A. Muralidhar, D. R. Tree, Y. Wang, and K. D. Dorfman, J. Chem. Phys. **140**, 084905 (2014).
[16] A. Muralidhar, D. R. Tree, and K. D. Dorfman, Macromolecules **47**, 8446 (2014).
[17] Y. Kim, K. S. Kim, K. L. Kounovsky, R. Chang, G. Y. Jung, J. J. dePablo, K. Jo, and D. C. Schwartz, Lab Chip **11**, 1721 (2011).
[18] P. Utko, F. Persson, A. Kristensen, and N. B. Larsen, Lab Chip **11**, 303 (2011).
[19] K. Frykholm, M. Alizadehheidari, J. Fritzsche, J. Wigenius, M. Modesti, F. Persson, and F. Westerlund, Small **10**, 884 (2014).
[20] E. Werner, F. Westerlund, J. O. Tegenfeldt, and B. Mehlig, Macromolecules **46**, 6644 (2013).
[21] L. Dai, J. van der Maarel, and P. S. Doyle, Macromolecules **47**, 2445 (2014).
[22] E. Werner and B. Mehlig, Phys. Rev. E **90**, 062602 (2014).
[23] A. Y. Grosberg and A. R. Khokhlov, *Statistical Physics of Macromolecules* (AIP Press, New York, 1994).
[24] T. W. Burkhardt, Y. Yang, and G. Gompper, Phys. Rev. E **82**, 041801 (2010).
[25] J. Z. Y. Chen, Macromolecules **46**, 9837 (2013).
[26] P. J. Flory, *Principles of Polymer Chemistry* (Cornell University Press, Ithaca, 1953).
[27] L. Turban, J. Phys. **45**, 347 (1984).
[28] See Supplemental Material at http://link.aps.org/supplemental/10.1103/PhysRevE.91.050601 for brief discussions of regime III and the scaling regimes of a polymer confined to a slit, as well as a table summarizing the predictions for all scaling regimes of Fig. 1.
[29] P. G. De Gennes, Macromolecules **9**, 587 (1976).
[30] L. Onsager, Ann. N. Y. Acad. Sci. **51**, 627 (1949).
[31] Z. Benková, P. Námer, and P. Cifra, Soft Matter **11**, 2279 (2015).
[32] F. Brochard and P. G. de Gennes, J. Chem. Phys. **67**, 52 (1977).
[33] B. Li, N. Madras, and A. D. Sokal, J. Stat. Phys. **80**, 661 (1995).
[34] E. F. Casassa, J. Polym. Sci., Part B: Polym. Lett. **5**, 773 (1967).
[35] A. Khorshid, P. Zimny, D. Tétreault-La Roche, G. Massarelli, T. Sakaue, and W. Reisner, Phys. Rev. Lett. **113**, 268104 (2014).